Theoretical and Applied Climatology (2022) 149:1373–1390
https://doi.org/10.1007/s00704-022-04096-3

ORIGINAL PAPER

The effects of the climatic change on daily maximum and minimum temperatures along 102 years (1917–2018) recorded at the Fabra Observatory, Barcelona

X. Lana[1] · C. Serra[1] · M. D. Martínez[1]

Received: 1 October 2021 / Accepted: 14 May 2022 / Published online: 15 June 2022

Abstract
Time trends and their statistical significance for daily minimum, Tmin, and maximum, Tmax, temperatures recorded at the Fabra Observatory (Barcelona) along 102 years (1917–2018) permit to analyse the evolution of every one of the 365 calendar days along the recording period. Relevant changes in the daily temperature regime have been quantified not only by time trends and the Mann–Kendall test, but also by the multifractal analysis applied to consecutive segments of daily temperature data. The evolution of several multifractal parameters (the central Hölder exponent, the spectral asymmetry and spectral amplitude, the complexity index and the Hurst exponent) provides a complementary viewpoint to describe the evolution of the thermometric regime along the 102 recorded years. At monthly scale, the effects of the climate change are characterised by significant positive trends from September to December and very moderate negative trends from April to July. With respect to changes in the calendar-day structure, it is noticeable a shift of the highest minimum and maximum daily temperature from July to August (year 2018) to the beginning of September (projections for years 2030 and 2050) and the projected highest maximum calendar-day temperature exceeding 30 °C.

1 Introduction

The effects on climate at local, regional and global scales of the anthropogenic climate change are nowadays unquestionable (Le Treut et al. 2007; Founda 2011; Hao et al. 2021; La Sorte et al. 2021; IPCC 2021), and changes in the frequency and duration of extreme climate events are pointed out (Diffenbaugh et al. 2017; Aghakouchak et al. 2020). From the viewpoint of thermometric regimes, it is worth highlighting the effects on the occurrence of extreme hot and cold events (Burgueño et al. 2002; Lana et al. 2009; Wheeler et al. 2011; Coumou and Robinson 2013). Additionally, the likely increase in length and intensity of heatwaves (Amengual et al. 2014; Russo et al. 2015; Lorenzo et al. 2021, among others), whose impacts could be exacerbated in large cities and metropolitan areas due to the urban heat island (UHI) effect has relevant concerns for human health, agriculture and forest fire risk (Bensoussan et al. 2010; Pausas and Fernández-Muñoz 2012; Smith and Sheridan 2019). Nowadays, it is widely accepted that emissions of CO_2 and other greenhouse gases (GHGs) into the atmosphere are affecting the temperature regime at global, regional and local scales (Bloomfield 1992; Stern and Kaufmann 2000; Jones and Moberg 2003; Sigró et al. 2005; Gil-Alana 2009; Gil-Alana and Sauci 2019; IPCC 2022), and the annual evolution of global average atmospheric concentration of CO_2 has been updated and published a few years ago by Meinshausen et al. (2017). The effects of GHG emissions on temperature regime changes have been studied from several points of view. Among many other researches, it could be cited Wigley and Santer (2013) who studied the role played by the CO_2 anthropogenic component along the twentieth century; Zickfeld et al. (2016) focused on the behaviour of temperature changes during periods of negative CO_2 emissions and more recently Agliardi et al. (2019) who have analysed the relationship between GHGs and global temperature anomalies. Consequently, a detailed knowledge at local scale of changes in the thermometric regimes is also of great interest.

✉ X. Lana
francisco.javier.lana@upc.edu

C. Serra
carina.serra@upc.edu

M. D. Martínez
dolors.martinez@upc.edu

[1] Departament de Física, Universitat Politècnica de Catalunya (UPC), Barcelona, Spain

In the present research, a long-term high-quality database of daily maximum and minimum temperatures recorded at Fabra Observatory (Barcelona, NE Spain) along the 1917–2018 period (102 years), without any lack of data, has permitted investigating the evolution of the multifractal structure of the daily temperatures, as well as a thorough analysis of the 365 calendar-day temperature pattern and its time evolution. The results, showing clear evidences of notable changes in the calendar-day structure of maximum, minimum and extreme temperatures, should contribute to improving the prospective knowledge of the thermometric regime in the Western Mediterranean region (Kutiel and Maheras 1998; Corte-Real et al. 1995; Xoplaki et al. 2003; Martínez et al. 2010; Gonçalves et al. 2014 and Barrera-Escoda et al. 2014, among others).

The contents of this paper are organised as follows. Section 2 explains the data quality of the maximum and minimum daily temperatures recorded at Fabra Observatory and offers a first overview of the thermometric regime at annual scale. Section 3 describes the MFDA multifractal algorithm and the obtained results, which evaluate the complexity of the temperature evolution for the whole data series and for consecutive segments of the series, thus permitting to derive the time evolution of this complexity since the beginning of the twentieth century up to nowadays. The evolution of the maximum and minimum calendar-day temperatures along the 102-years recording period is examined in detail in Sect. 4, the likely projections of the calendar-day profile for years 2030 and 2050 being then derived. The results of this thermometric analysis are discussed in Sect. 5, and Conclusions, in Sect. 6, summarises the most relevant results concerning future changes in the temperature regime, which would possibly affect Barcelona city and its metropolitan area.

2 Database

The daily database for the detailed analysis of the evolution of the thermometric regime at daily, monthly, seasonal and annual scales in Barcelona has been obtained from the Fabra Observatory, owned by the Royal Academy of Art and Sciences of Barcelona. Figure 1 shows the location of the observatory. It is placed on the littoral chain at a moderate altitude of 415 m.a.s.l. and a few kilometres from the Mediterranean shoreline. Although placed within the municipality of Barcelona, it is out of the urban continuum. This database is notably long, without any gap all along the 102-year period considered (1917–2018), and of high quality and homogeneity (Serra et al. 2001; Burgueño et al. 2014; Lana et al. 2015), verified by AEMET (Spanish Meteorological Agency), SMC (Meteorological Service of Catalunya, www.meteo.cat) and also available in European Climate Assessment & Dataset (www.ecad.eu). The last day of February in leap years has been removed for avoiding the low time trend reliability for this specific calendar day. Whereas only 25 samples are available for February 29th, 102 samples for every one of the other 365 calendar days permit a much more accurate computation. It is also assumed that, at monthly, seasonal and annual scales, removing this calendar day would represent a

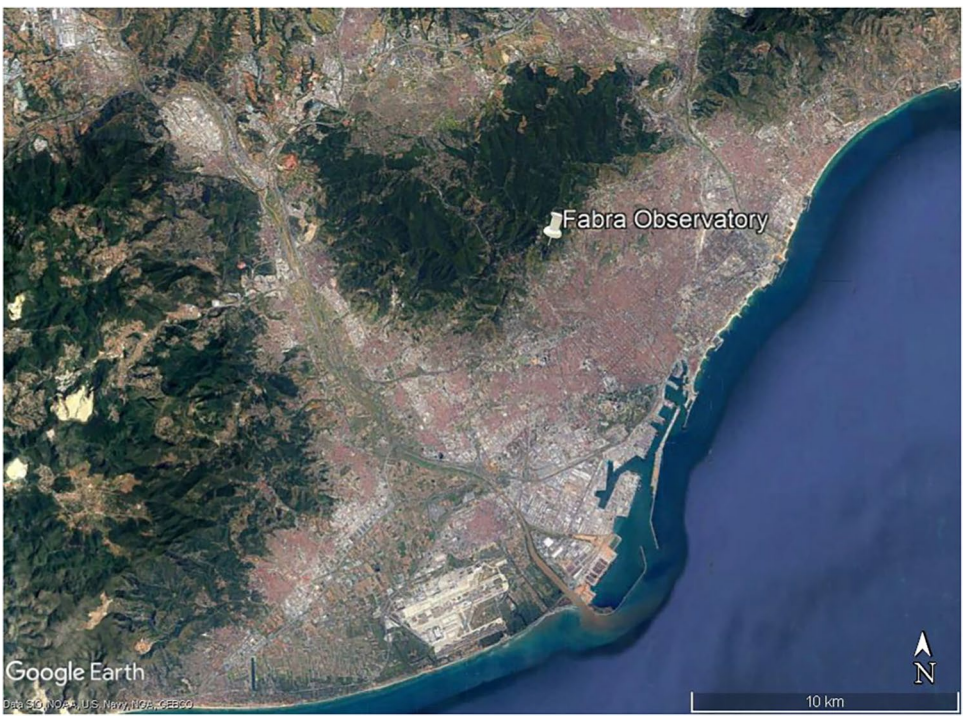

Fig. 1 Location of the Fabra Observatory in the metropolitan area of Barcelona

very small perturbation on the computed time trends. Consequently, time trends of temperature regime and their statistical significance can be conveniently analysed.

A first description of the maximum, Tmax, and minimum, Tmin, temperatures is depicted in Fig. 2a and b, where the running average of 365 samples' length of maximum and minimum daily temperatures and their average, extreme and standard deviation for every calendar day have been represented. In agreement with Fig. 2a, a relevant change on the tendency of both temperatures, with some time lag between them, is detected. Running average of maximum temperatures depicts fluctuations approximately between 16.5 and 19.5 °C up to the beginning of the 1970s decade. Afterwards, a notable increasing evolution is observed, being achieved oscillations from 19.5 to 21 °C along the last three decades. Running average of minimum temperatures depicts a similar pattern with an increasing tendency detected at the end of the 1970s decade, a few years delayed with respect to maximum temperatures. Whereas minimum average temperatures fluctuate between 10.0 and 12.0 °C up to the end of 1970s decade, since the end of the twentieth century, they oscillate within an interval close to 11.5–13.5 °C. With respect to the distribution of the recorded temperatures along the 365 calendar days (Fig. 2b), the best fits (the lowest RMSE) of average and extreme minimum and maximum temperatures are obtained with fifth-degree polynomials, being noticeable several days with Tmax exceeding 35 °C (some of them very close to 40 °C) for July and August, and other days since December to February with Tmin lowering 0 °C, in a few cases close to − 10 °C. It has to be also mentioned that the standard deviation of the calendar-day extreme temperatures ranges between 2.5 and 4.0 °C for Tmax and from 2.1 to 3.9 °C for Tmin, then suggesting a little larger fluctuation for extreme maximum temperatures.

3 Multifractal structure of daily temperatures

The degree of multifractal complexity is quantified by the multifractal detrended fluctuation analysis, MDFA (Kantelhardt et al. 2002), which has been applied, among other scientific fields, to geosciences data series — seismology (Aggarwal et al. 2015; Fan and Lin 2017 and Monterrubio-Velasco et al. 2020, among others) — and climatology analyses (Burgueño et al. 2014; and Lana et al. 2020, among others). In this research, this algorithm is applied to a high number of maximum and minimum daily temperatures (more than 37,000 daily data), hence being assured a good accuracy of the results. The same algorithm is also applied to segments of daily data (moving windows), thus permitting an analysis of the multifractal evolution of the thermometric regime since 1917 up to 2018. A detailed description of the computational steps of the MDFA algorithm can be found, among others, in Burgueño et al. (2014).

The multifractal spectrum, F(α), can be computed as

$$F(\alpha) = A(\alpha - \alpha_0)^2 + B\left(\alpha - \alpha_0\right) + C \tag{1}$$

$$\alpha(q) = h(q) + qdh(q)/dq \tag{2}$$

$$F_{s(q)} \approx s^{h(q)};(q = -qmin, \ldots, 0, \ldots, qmax \tag{3}$$

This multifractal spectrum is based on α, the Hölder exponent, three coefficients (C, theoretically equal to 1.0, and A and B), all of them obtained by means of a second-order polynomial fit of empiric F(α), and the central Hölder exponent α_0, accomplishing $F(\alpha_0) = 1.0$. Equation (2) establishes the relationship between the Hölder exponent α(q) and the generalised Hurst exponent, h(q), and Eq. (3) represents the q-order fluctuation function, $F_s(q)$, of the different data segments, S(q), analysed, then being obtained the generalised Hurst exponent h(q). This generalised exponent will be equal to the usual Hurst exponent, H, for q = 2 when stationary time series are analysed. Alternatively, for non-stationary or noisy series, H will be equal to h(q = 2) − 1.0.

The fit of empirical multifractal spectrum data to Eq. (1) permits to obtain the extreme α_{MAX} and α_{MIN} Hölder exponents accomplishing $F(\alpha_{MAX}) = F(\alpha_{MIN}) = 0$; the spectral amplitude, $W = \alpha_{MAX} - \alpha_{MIN}$; and the spectral asymmetry, $\gamma = (\alpha_{MAX} - \alpha_0)/(\alpha_0 - \alpha_{MIN})$, which could vary from total symmetry (γ = 1.0) to high right (γ > > 1.0) or high left (γ < < 1.0) asymmetries. Standardised values of α_0, W and γ for every data segment are used to obtain the evolution of a complexity index, CI (Shimizu et al. 2002), of the analysed series. This index CI is computed by adding the standardised values of W, γ and α_0. Additionally, the usual Hurst exponent, H, will quantify the degree of persistence ($H > 0.5$), anti-persistence ($H < 0.5$) or randomness ($H \approx 0.5$) of the analysed series.

The results of the multifractal analysis applied to the complete daily data are shown in Fig. 3a, b and c. As expected, α(q) diminishes for increasing values of q-order. The Hurst exponent, both for maximum and minimum daily temperature series, is characterised by notable signs of randomness (values close to 0.5) and the parameter $\tau = qh(q) - 1$, leading to Eq. (2) (bearing in mind that $\alpha(q) = d\tau/dq$) also depicts a high similarity between maximum and minimum temperature series. The multifractal polynomial (Fig. 4) shows some differences, with respect to the spectral amplitude, when comparing Tmax (0.47 units) and Tmin (0.64 units) series. From this point of view, Tmin series would be a bit more complex than Tmax series. Some shortcomings have to be also mentioned. First, for both multifractal computations, empiric

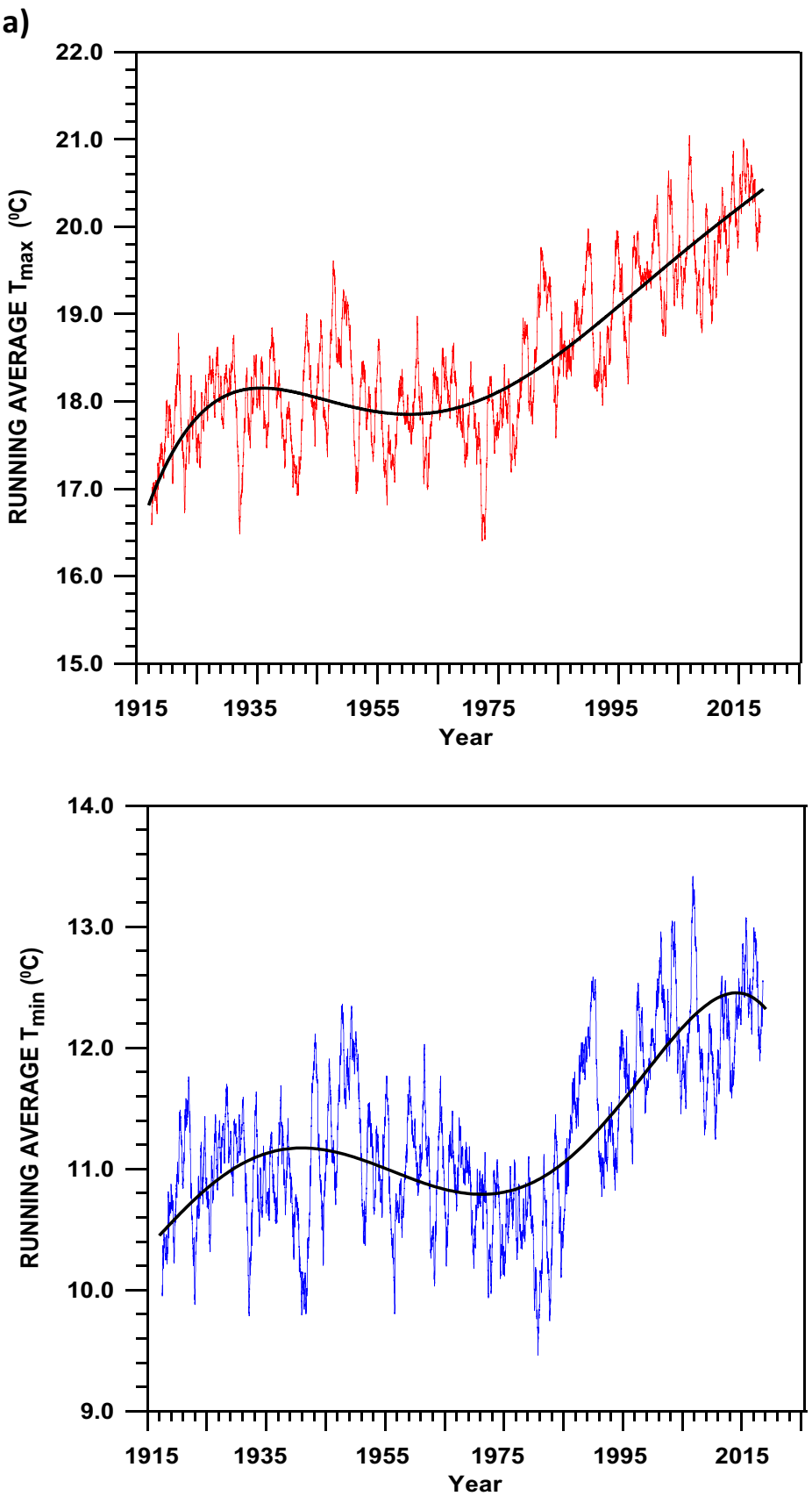

Fig. 2 **a** Running average of the maximum and minimum temperatures. **b** Average, extreme temperatures and standard deviations for every calendar day (years 1917–2018)

Fig. 2 (continued)

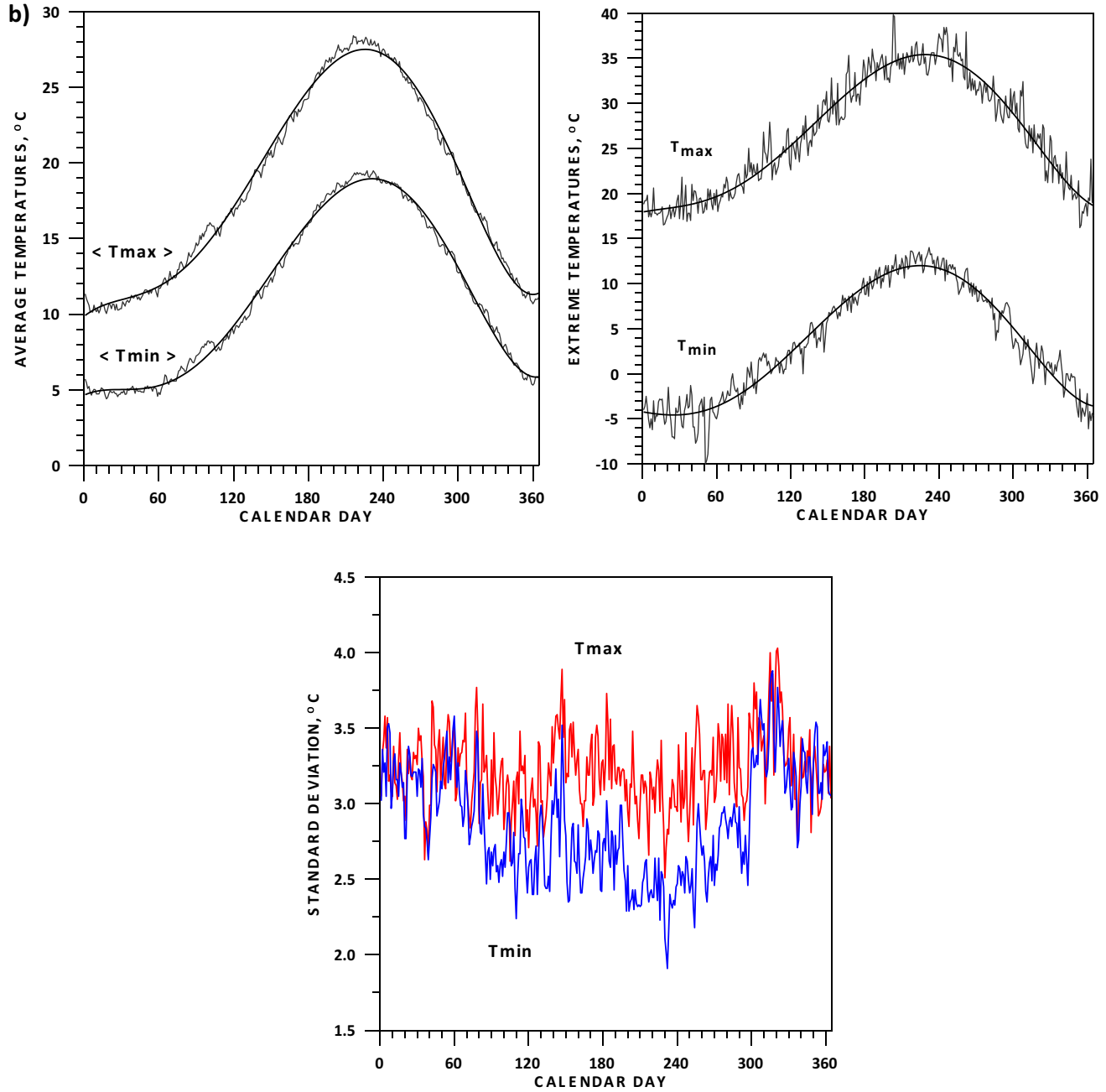

central Hölder exponents are not exactly coincident with those deduced from the polynomial fit. Second, uncertainties on the extreme Hölder exponents are also observed, given that sometimes empiric multifractal amplitudes close to 0, defining extreme $q_{\min}$ and $q_{\max}$, depart from Eq. (1) and cannot be used for a more accurate quantification of coefficients A and B. Then, extreme Hölder exponents, α_{MAX} and α_{MIN}, are determined with some small uncertainty and the asymmetry, and spectral amplitude, both concerning the complexity index, could be also submitted to some uncertainty. Results would suggest that it could affect slightly more to Tmin in comparison with Tmax. Nevertheless, this difference is negligible, taking into account the computational uncertainty.

The same multifractal algorithm has been applied to moving windows of 25-year length, every time shifted 5 years, then obtaining several samples of the multifractal evolution along 102 years. Figure 5a depicts a clear decreasing evolution of the central Hölder exponent for Tmax and Tmin. Not so clear negative trends are observed for the evolution of

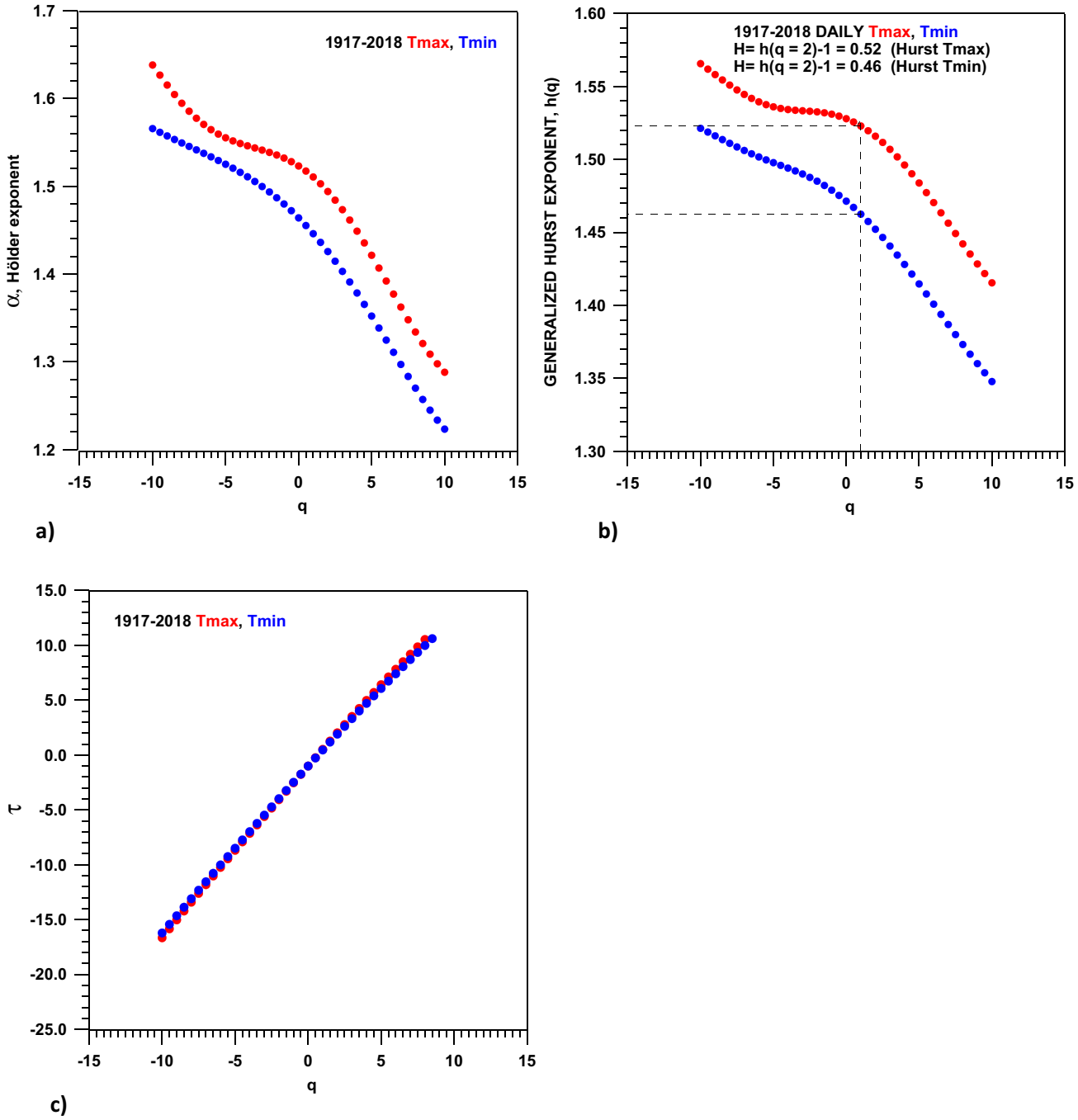

Fig. 3 **a** Hölder exponent, α(q), of the multifractal analyses; **b** generalised Hurst exponent, h(q); and **c** τ(q) exponent for the maximum and minimum daily temperature series

the asymmetry (Fig. 5b), except for Tmax since 1980, and decreasing trends are clearly detected only for the spectral amplitude (Fig. 5c) since approximately 1995 up to 2018. Given that the generalised Hurst values h(q) of the multifractal structure exceed 1.0, the usual Hurst exponent H has to be computed as h(q = 2) – 1.0. The evolution of this exponent (Fig. 5d) also decreases up to 2001, very moderately changing to positive trends since 2001 to 2018. It is definitively observed that, in spite of this change in the time trends, both thermometric series are characterised by a random behaviour, with H equal to h(q = 2) – 1.0 varying within a narrow fringe from 0.44 to 0.55, thus being discarded up to nowadays changes from randomness to persistence or antipersistence. Only analyses of future temperature data could verify if these new trends persist and the multifractal structure will change from randomness to persistence. Finally,

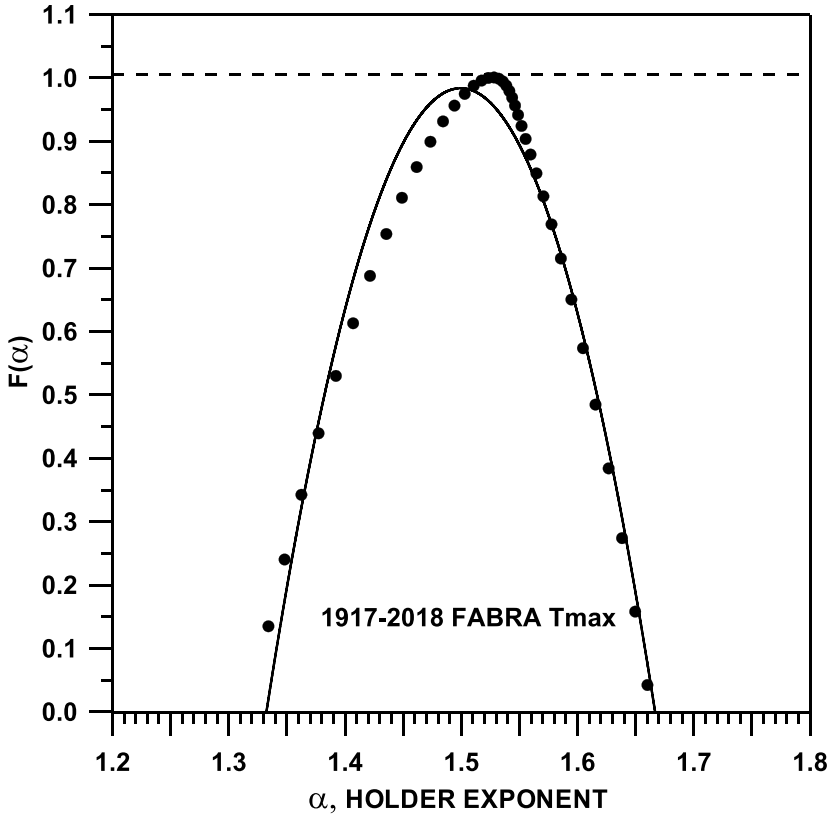

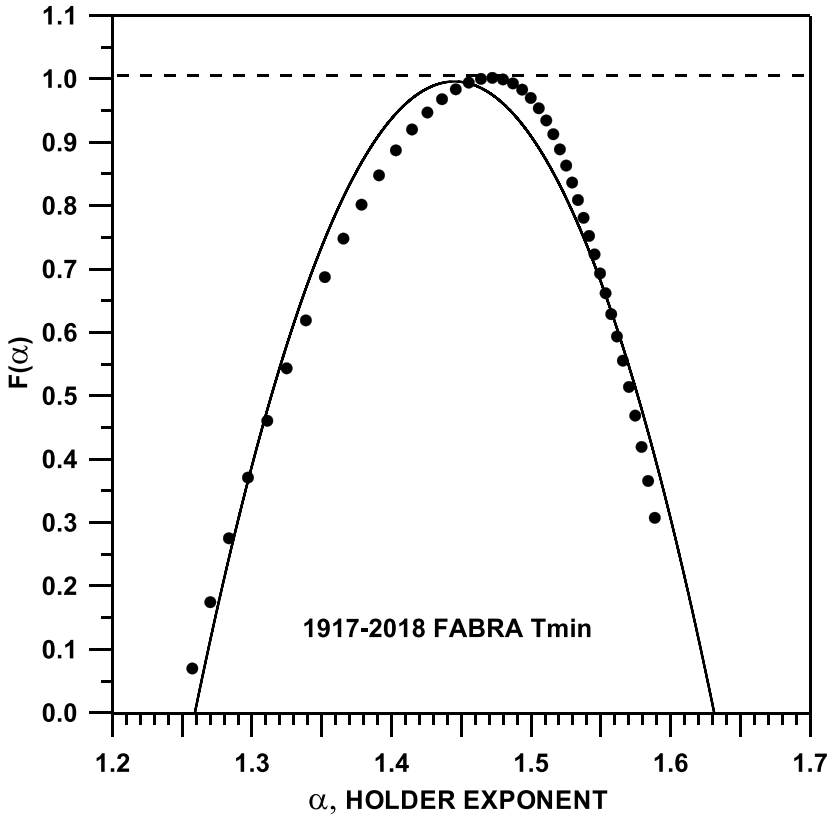

Fig. 4 Multifractal spectra for the whole series of maximum and minimum temperatures

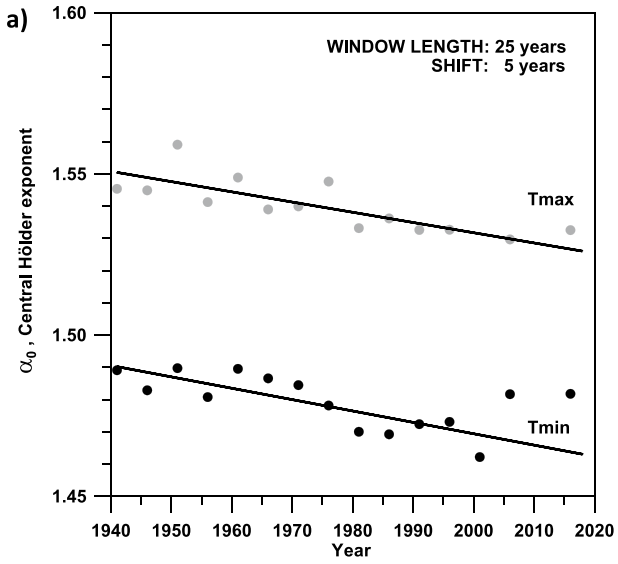
a)
WINDOW LENGTH: 25 years
SHIFT: 5 years
Tmax
Tmin
α_0 , Central Hölder exponent
Year

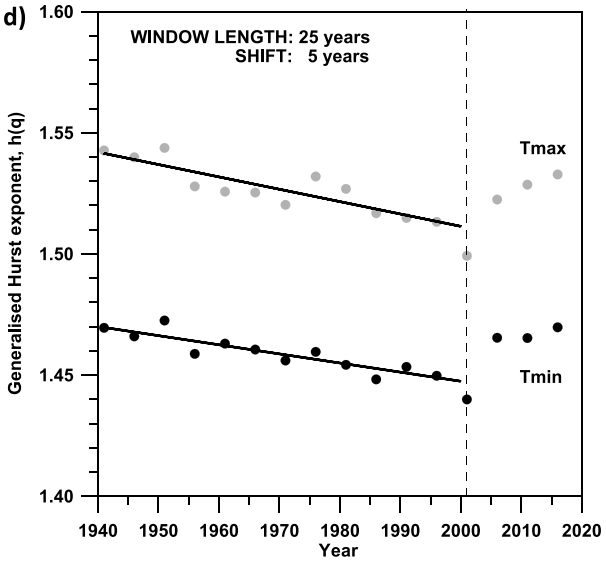
d)
WINDOW LENGTH: 25 years
SHIFT: 5 years
Tmax
Tmin
Generalised Hurst exponent, h(q)
Year

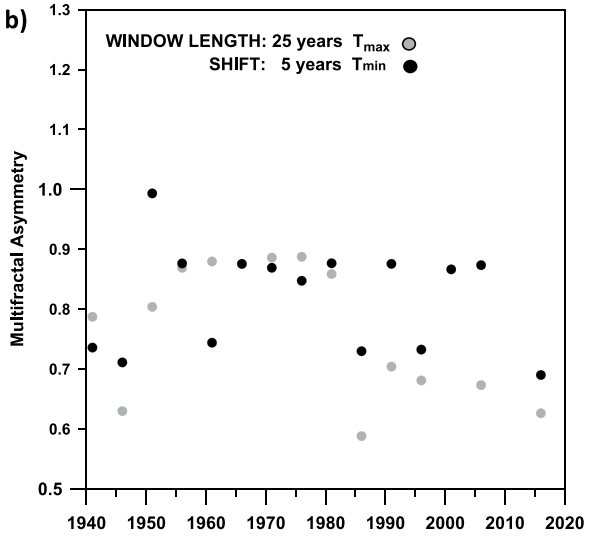
b)
WINDOW LENGTH: 25 years T_{max}
SHIFT: 5 years T_{min}
Multifractal Asymmetry

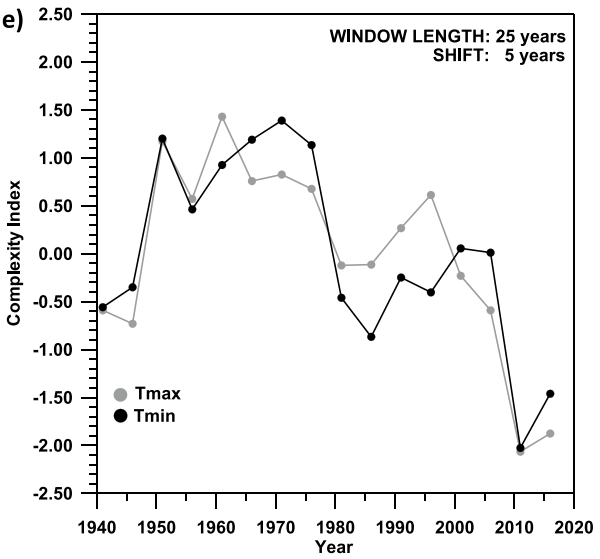
e)
WINDOW LENGTH: 25 years
SHIFT: 5 years
Tmax
Tmin
Complexity Index
Year

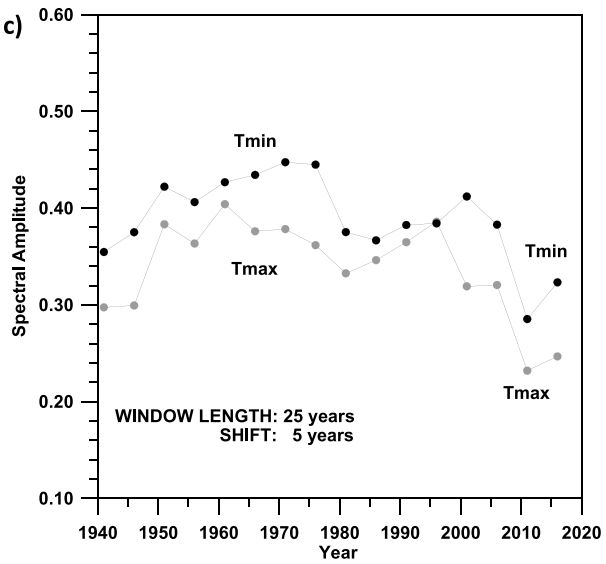
c)
Tmin
Tmax
Tmin
Tmax
WINDOW LENGTH: 25 years
SHIFT: 5 years
Spectral Amplitude
Year

◂**Fig. 5** Evolution of **a** Central Hölder exponent, α_0; **b** multifractal asymmetry, γ; **c** spectral amplitude, W; **d** Hurst exponent, $H = h(q=2) - 1.0$; and **e** complexity index, CI, for moving windows of 25-year length and 5-year shift

the degree of complexity (Fig. 5e) depicts an outstanding reduction from year 1970 (+1.50 for Tmin and +0.75 for Tmax) to year 2018 (−1.50 for Tmin and −2.00 for Tmax).

In agreement with the detected time trends on multifractal parameters, a single-time evolution for the whole set of parameters is not detected, and it is also evident that the parameter CI, quantifying the degree of complexity, clearly decreases since 1970, and the Hurst exponent, in spite of a clear change from negative to positive trend, is associated up to nowadays with randomness, instead of persistence ($H > > 0.5$) or anti-persistence $H < < 0.5$).

4 Calendar-day characteristics and temperature trends

Daily maximum and minimum temperature trends for the 365 calendar days have been computed and their statistical significance evaluated by means of the Mann–Kendall test (Sneyers 1990). A detailed description of the evolution of the daily maximum and minimum temperatures is summarised in Table 1 and Fig. 6. As observed in this figure, most of time trends are positive, for both daily Tmax and Tmin, and are especially high in autumn. The corresponding Mann–Kendall percentage of statistical significance depicts a quite similar evolution, being relevant that statistical significances equalling or exceeding 99% are clearly dominant in autumn. Time trends and the Mann–Kendall test results for every calendar day have been grouped into the corresponding month and season (Table 1). This procedure permits a description of variability at monthly and seasonal scales, based on the 102 samples for every calendar day guaranteeing the accuracy of the results. Extreme maximum and minimum time trend variability, as well as average and standard deviations at monthly and seasonal scales, is then obtained, taking advantage of the confident time trends derived for the 365 calendar days. The 365 Mann–Kendall tests and time trend values have also been used to detect the time trend diversity of maximum and minimum temperatures at annual scale. The results clearly reveal positive Mann–Kendall values, very often exceeding 90% of statistical significance (empiric Mann–Kendall parameter equalling to or exceeding 1.64), accompanied by averaged high positive time trends, especially for January and from August to December, for both maximum and minimum temperatures. The maximum temperatures from August to December depict the highest positive averaged trends, reaching 7.4 °C per century in November. The minimum temperatures show remarkable positive trends for January and from September to December, although more moderate than maximum temperatures. The largest positive trend is attained again in November (5.9 °C per century). At seasonal scale, the time trends are smoothed due to the different behaviour of consecutive calendar days pertaining to the same season. Nevertheless, most of time trends are positive (except for maximum temperatures in spring), and it is worth highlighting the outstanding positive trends for maximum (6.2 °C/century) and minimum (4.5 °C/century) temperatures in autumn. At annual scale, these high positive trends are notably smoothed due to the moderate contribution of winter, summer and spring, in comparison with autumn. Average time trends at annual scale leading to possible increases of 2.4 °C (maximum temperatures) and 1.4 °C (minimum temperatures) along 100 years could be considered as a troubling effect of the human-induced climate change.

In agreement with Table 1 and Fig. 6, the time behaviour of maximum and minimum calendar-day temperatures is not homogeneous along the year. As an example, the calendar-day patterns of maximum and minimum temperatures corresponding to years 1920 and 2018 (at the beginning and the end of the recording period) are represented in Fig. 7, jointly with 6th degree polynomial fits (thick lines). More than relevant temperature differences for some specific calendar days among these two years separated by almost a century, polynomial fits permit observing larger increases in Tmax and Tmin for the second half of the year than for the first half, reaching around +3.5 °C (Tmax) and +2.0 °C (Tmin) at the beginning of August. In the year 2018, a slight shift to the right of the peak for Tmax is suggested. These patterns are compared with prospective calendar-day temperatures derived for years 2030 and 2050, based on time trends computed for each calendar day (Fig. 8). Looking at the 6th degree polynomial fits (thick lines), besides the increment of temperature levels, the changes in the calendar-day structure are outstanding, with a clear displacement to the end of summer of the maximum calendar-day temperatures.

As an example of the different behaviour of every calendar day, Fig. 9 shows the evolution of maximum and minimum temperatures, all along the recording period, for three selected calendar days (June 13th, September 7th and November 10th). The observed evolution is in agreement with the expected displacement, along the next decades, of extreme maximum and minimum temperatures from summer to autumn, as indicated in Fig. 8. Accompanying the temperature oscillations, linear fits suggest clear time trends associated to Tmax and Tmin for the three calendar days considered. For June 13th, the slopes of linear fits are negative and quite similar for Tmax and Tmin. For September 7th and November 10th, both slopes are positive, slightly larger

Table 1 Variability at monthly, seasonal and annual scales of maximum, minimum, average and standard deviation of temperature time trends, TRD, (°C/year) and Mann–Kendall, MK, parameter. The highest minimum, maximum and average positive time trends are distinguished (shaded cells). All absolute values of minimum, maximum and average and standard deviation of MK parameters exceeding to or equalling 90% of statistical significance are also highlighted in bold types

Tmax	MinTRD	MaxTRD	<TRD>	σ(TRD)	minMK	maxMK	<MK>	σ(MK)
January	0.019	0.048	0.031	0.008	**1.66**	**4.46**	**2.71**	0.72
February	-0.001	0.035	0.015	0.009	-0.51	**2.76**	1.13	0.82
March	-0.021	0.017	-0.001	0.009	**-1.91**	1.46	0.20	0.88
April	-0.019	0.023	-0.012	0.011	**-2.07**	**2.21**	0.02	1.11
May	-0.028	0.006	-0.018	0.008	**-2.55**	1.00	-1.09	0.72
June	-0.038	0.002	-0.018	0.011	**-4.08**	-0.15	**-1.75**	1.00
July	-0.029	0.019	-0.001	0.013	**-2.37**	**1.79**	-0.14	1.12
August	-0.002	0.060	0.028	0.016	-0.04	**5.22**	**2.77**	1.46
September	0.034	0.073	0.051	0.009	**3.30**	**6.43**	**4.70**	0.80
October	0.051	0.090	0.066	0.009	**4.99**	**7.71**	**5.97**	0.63
November	0.057	0.096	0.074	0.010	**5.39**	**7.60**	**6.50**	0.55
December	0.037	0.064	0.047	0.008	**3.10**	**5.91**	**4.34**	0.81
Winter	-0.021	0.048	0.017	0.014	**-1.91**	**4.46**	1.35	1.32
Spring	-0.038	0.023	-0.010	0.013	**-4.08**	**2.21**	-0.94	1.19
Summer	-0.029	0.073	0.026	0.025	**-2.37**	**6.43**	**2.42**	2.30
Autumn	0.037	0.096	0.062	0.014	**3.10**	**7.71**	**5.59**	1.14
Annual	-0.038	0.096	0.024	0.031	**-4.08**	**7.71**	**2.12**	2.82
Tmin	**MinTRD**	**MaxTRD**	**<TRD>**	**σ(TRD)**	**minMK**	**maxMK**	**<MK>**	**σ(MK)**
January	0.013	0.043	0.028	0.008	0.73	**4.03**	**2.373**	0.774
February	-0.005	0.029	0.013	0.008	-0.76	**2.92**	0.97	0.81
March	-0.017	0.012	-0.005	0.008	**-1.75**	1.15	-0.52	0.76
April	-0.024	0.005	-0.004	0.010	**-2.30**	1.57	-0.44	1.09
May	-0.034	-0.009	-0.020	0.007	**-3.41**	0.81	**-2.26**	7.35
June	-0.037	-0.005	-0.022	0.110	**-4.50**	0.50	**-2.57**	1.06
July	-0.021	0.008	-0.005	0.009	**-2.67**	1.32	-0.70	1.16
August	-0.004	0.038	0.014	0.011	-0.67	**4.44**	**1.81**	1.31
September	0.014	0.051	0.029	0.009	1.29	**4.70**	**3.19**	0.89
October	0.025	0.075	0.040	0.009	**2.85**	**6.18**	**3.85**	0.75
November	0.035	0.069	0.059	0.013	**3.29**	**6.44**	**5.12**	0.97
December	0.027	0.056	0.037	0.006	**2.17**	**4.81**	**3.28**	0.60
Winter	-0.017	0.043	0.012	0.016	**-1.75**	**4.03**	0.94	1.44
Spring	-0.037	0.015	0.015	0.012	**-4.50**	1.57	**-1.76**	1.37
Summer	0.025	0.065	0.004	0.009	**2.85**	**6.18**	**3.85**	0.35
Autumn	0.025	0.079	0.045	0.013	**-2.17**	**6.44**	**4.07**	1.09
Annual	-0.037	0.079	0.014	0.026	**4.50**	**6.44**	1.17	2.56

for Tmax than for Tmin. In terms of the absolute values of time trends, the most relevant change in temperatures for these three examples corresponds to November 10th.

An additional interesting picture of the expected changes in thermometric regime is provided by Fig. 10, where the annual values of TMAX(max) and TMAX(min) (extreme maximum temperatures) and TMIN(max) and TMin(min) (extreme minimum temperatures), all along the recording period, are displayed. Continuous and dashed thick lines represent, respectively, third-degree polynomial fits and 11-year running average. In all cases, the profiles are characterised by notable oscillations and increasing trends. The extreme TMAX(max) values range between 30 and 38 °C, with an increasing tendency

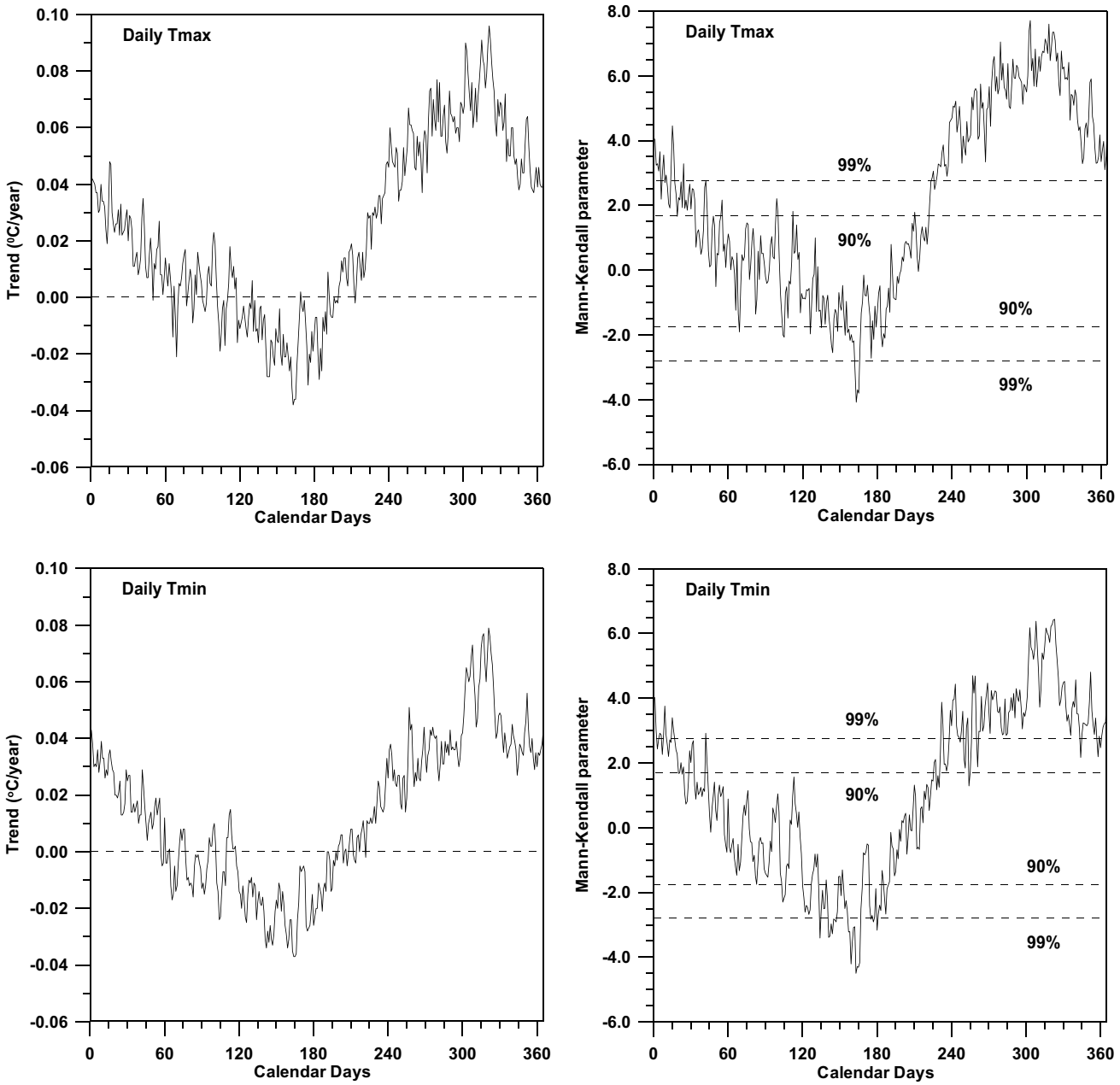

Fig. 6 Calendar-day time trends for maximum and minimum temperatures and the corresponding Mann–Kendall test percentages

suggested by the polynomial fit and confirmed by a linear trend of + 0.02 °C/year. The highest value close to 40 °C should not be taken into account, given that it was the result of a coincidence of a hot summer day (on account on the synoptic conditions), enhanced for a large forest fire very close to Barcelona city. The extreme TMIN(max) values depict a more moderate increasing tendency (linear trend of + 0.01 °C/year) and a high number of years with values exceeding 24 °C, which should be associated with urban heat island effects and/or heat waves lasting several days. Extreme TMAX(min) and TMIN(min) range from − 2 to 8 °C and from − 10 to 4 °C, respectively, with a linear trend of + 0.02 °C/year in both cases.

As a summary of the evolution of temperatures at calendar-day scale, it has to be taken into account that due to astronomical reasons (solstices and equinoxes are not coincident for every year) could be slightly more accurate to analyse time trends taking, for instance, as computational scale three consecutive calendar days instead of one single calendar day. Nevertheless, it is unlikely that the trend patterns derived for Tmax and Tmin calendar profiles would be significantly biased by this fact.

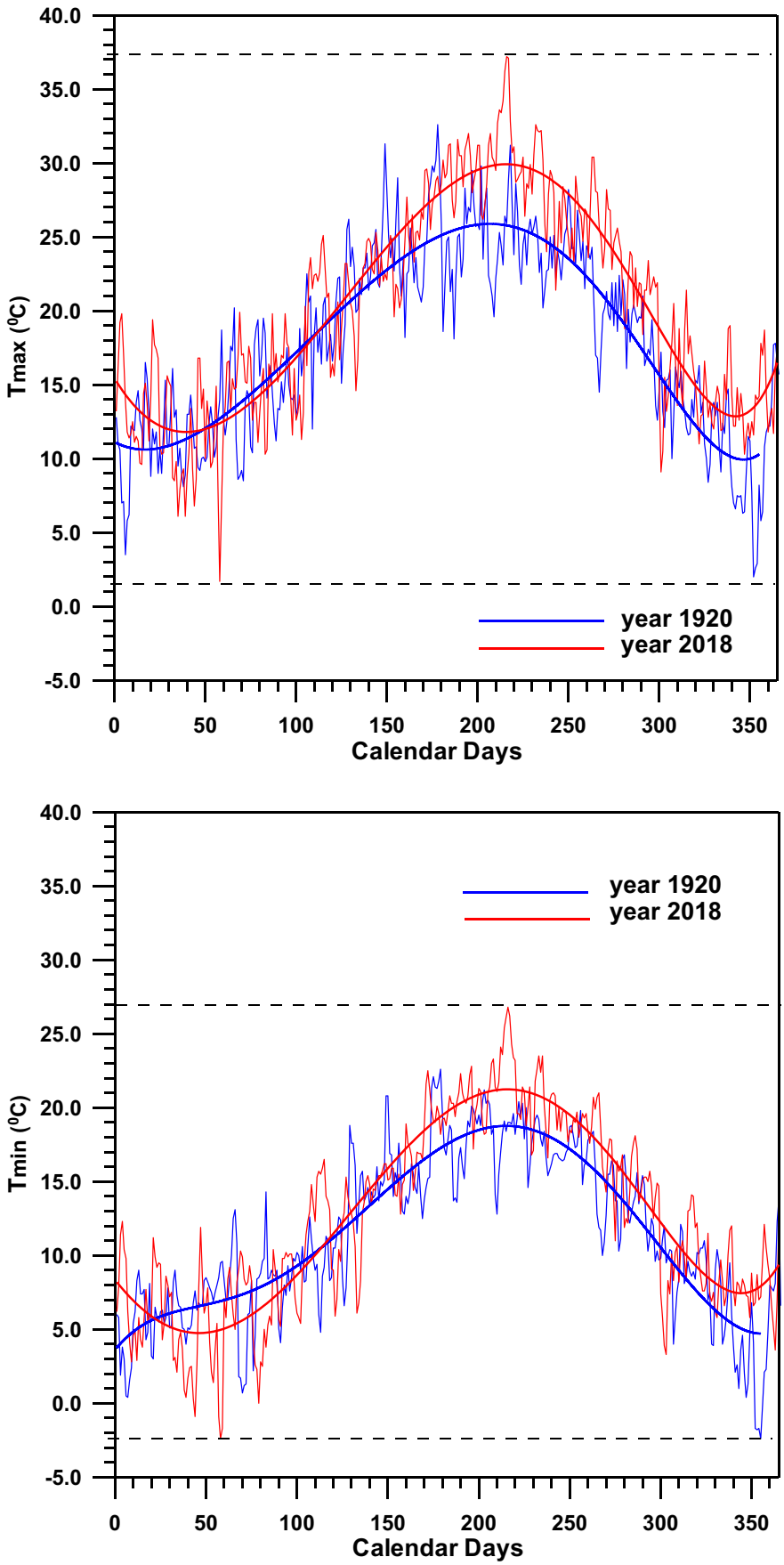

Fig. 7 Maximum and minimum calendar-day temperatures for years 1920 and 2018 (thin lines). Thick lines correspond to the 6th degree polynomials fits

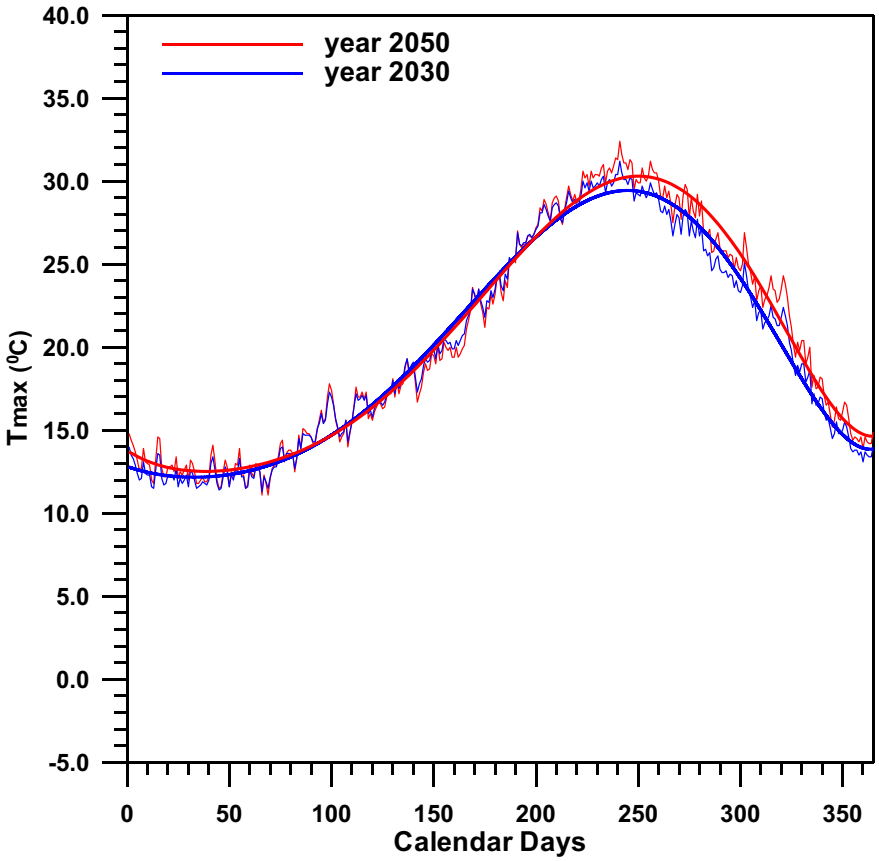

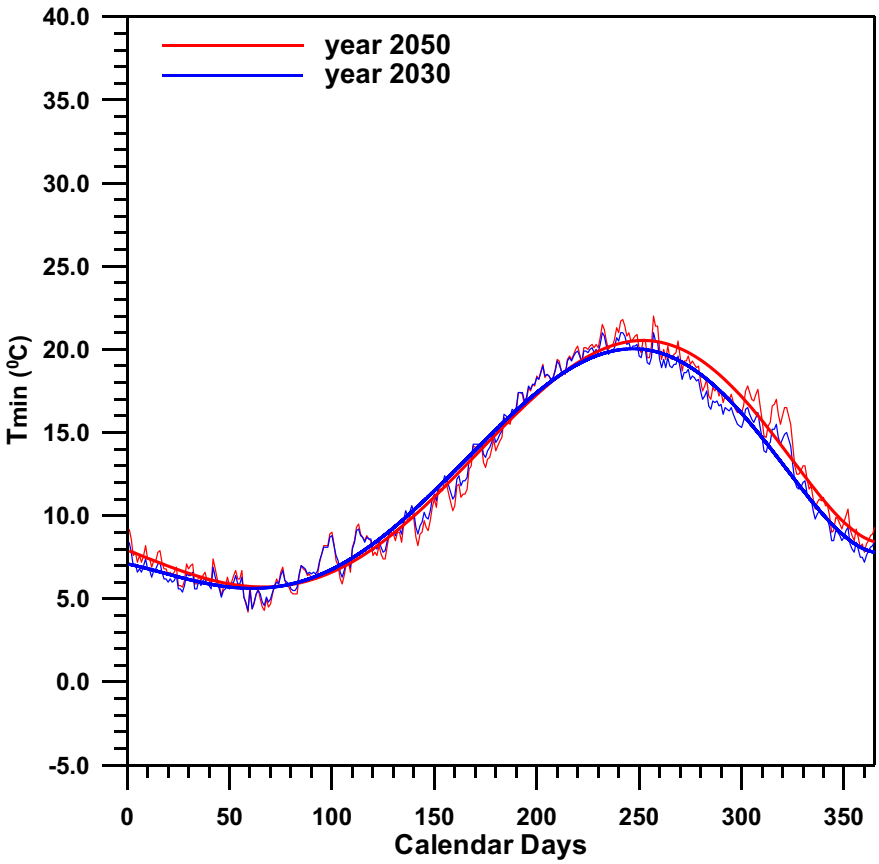

Fig. 8 Calendar-day maximum and minimum temperatures derived for years 2030 and 2050 taking as reference time trends detected for the 1917–2018 period

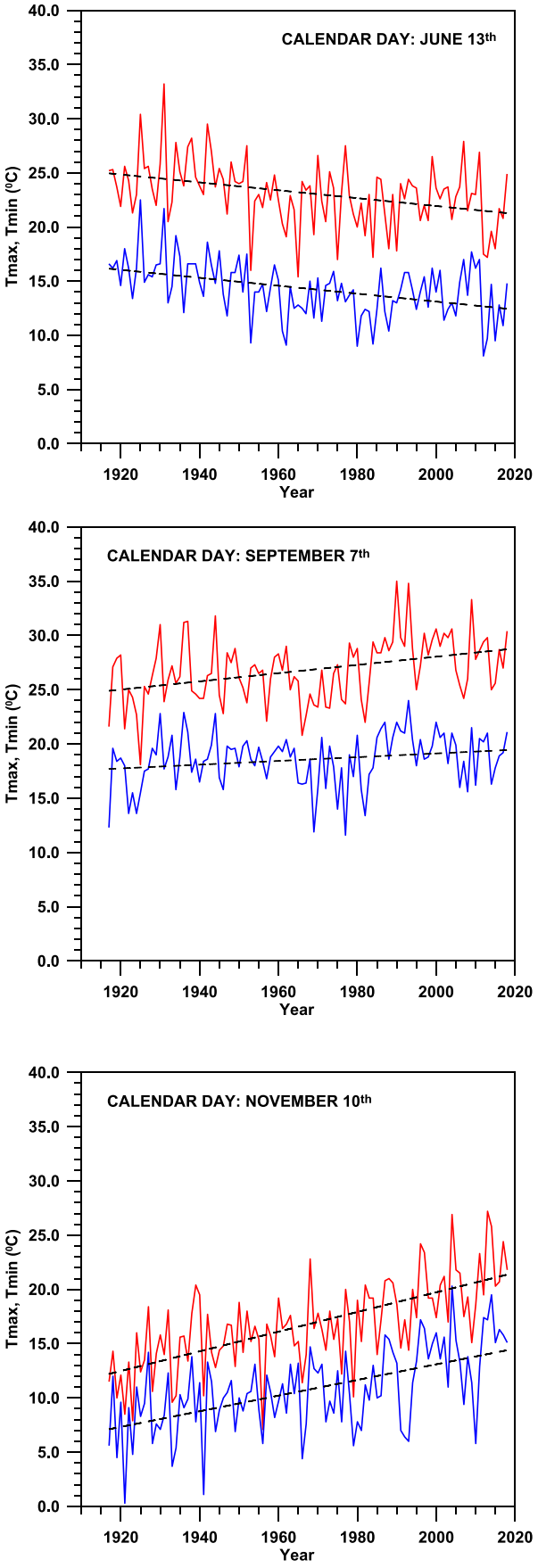

Fig. 9 Three examples of the evolution, all along the recording period, of maximum and minimum temperatures for June 13th, September 7th and November 10th calendar days

It should be also underlined two questions concerning these calendar profiles. By the one hand, the maximum Tmax and Tmin values are shifted along the years towards the end of summer and beginning of autumn, and this displacement of maximum temperatures is accompanied by an increase of temperatures for a high percentage of calendar days. These evolutions at annual scale would imply an overall increase of Tmax and Tmin and a displacement of the highest values to the end of summer. Consequently, it could be probable a future increase of temperatures for many calendar days and longer summers, both patterns compatible with some characteristics of the hotspot of the Mediterranean basin, which has been analysed from different points of view the last two decades (Diffenbaugh et al. 2007, 2012; Giannakopoulos et al. 2009; Paeth et al. 2017; Lionello et al. 2018; Tuel et al. 2020 and Cos et al. 2022, among others).

5 Discussion of the results

The long-term high-quality thermometric data of the Fabra Observatory (Barcelona) has permitted a detailed analysis of daily maximum and minimum temperature series along the period 1917–2018 (102 years). The results suggest forthcoming expected changes in the thermometric regime in the municipality of Barcelona and, probably, in the surrounding metropolitan area.

The observed and prospective changes in the thermometric regime of the Fabra Observatory could be expected to be influenced by the global warming induced by the increase in GHG emissions. Nevertheless, the enhancement of the UHI effect, because of the rise in population and the intense urbanisation process of the municipality of Barcelona and its metropolitan area along the last century, also would contribute to these thermometric changes. The population in the municipality of Barcelona city has increased from 530,000 inhabitants (year 1900) to 1,600,000 (year 2015), distributed on 100 km^2, and the whole metropolitan area houses around 3.2 million people (year 2015) in an area of 636 km^2. Due to the large population density and the compact urbanisation, the UHI phenomenon could be a non-negligible contribution to the changes detected in the temperature regime, especially for Barcelona city. Quereda et al. (2000) assumed that the increasing temperatures in cities of the Western Mediterranean coast depend more on the UHI phenomenon than on increases of CO_2 emissions. Additionally, Moreno-Garcia (1994), Salvati et al. (2017), Barros Pozo and Martín-Vide (2018) and Martín-Vide and Moreno-García (2020) confirm the

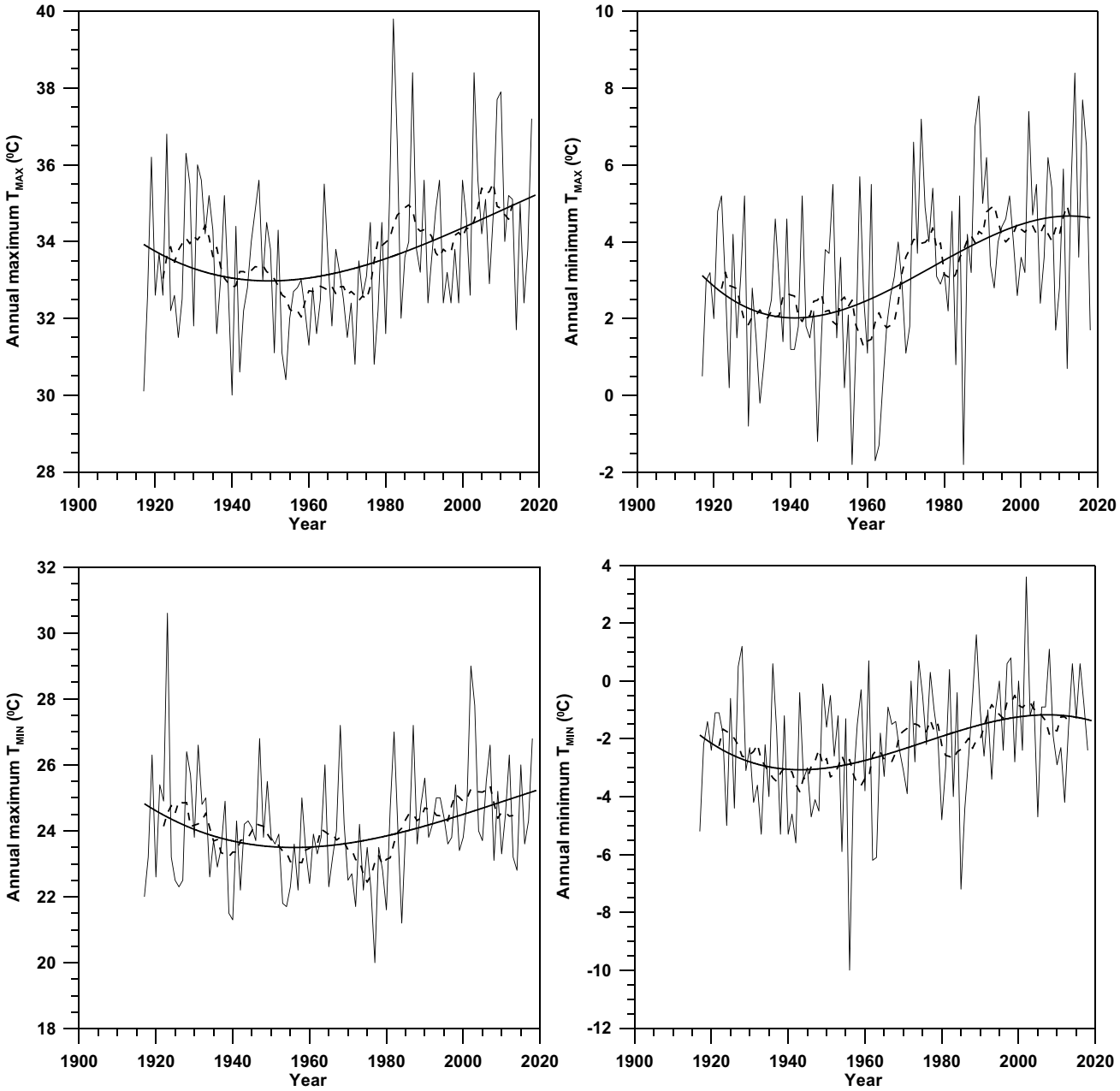

Fig. 10 Annual extreme maximum and minimum temperatures for the 1917–2018 period. Thin lines represent annual values, thick lines a third-degree polynomial fit and dashed lines running averages of 11 years

non-negligible influence of the UHI effect on the thermometric regime in Barcelona city. Additionally, Serra et al. (2020) detected the nuclei with the highest UHI intensity, for minimum temperatures, in the Barcelona metropolitan area by means of MODIS satellite and GIS data, several of them within Barcelona city. In spite of the non-negligible influence of the UHI effect in the temperature regime of the Fabra Observatory, this thermometric station would be the less affected among the stations in Barcelona city. The Fabra Observatory is at an altitude of 415 m.a.s.l. (Littoral Chain), surrounded of pine trees and away from buildings, out of the urban continuum.

The diversity of calendar-day time trends, including Mann–Kendall significance and many positive (and a few negative) time trends, together with projections performed for years 2030 and 2050, suggests forthcoming changes in the expected calendar-day profile. Homogeneous increments of maximum and minimum calendar-day temperatures are not expected along the year. The main change probably could be the shift of the climatic summer towards the

beginning of September and a general increase of Tmax and Tmin, quite different all along the year. The obtained results would be in agreement with temperature time trends (Gonçalves et al. 2014) and evolution of extreme temperatures (Barrera-Escoda et al. 2014) deduced for the North Western Mediterranean. Additionally, the results of this research could be validated by comparing them with the climate scenarios obtained for different areas of Catalonia (NE Spain) by Altava-Ortiz and Barreda-Escoda (2020).

The multifractal analysis by means of moving windows shows signs of an evolution towards a more simplified multifractal structure, manifested by a decreasing tendency of central Hölder exponents, both for Tmax and Tmin; the asymmetry of the multifractal spectra depicting negative trends, especially for Tmin; and the multifractal spectral amplitude, decreasing approximately after 1995, both for Tmax and Tmin. Additionally, the evolution of the multifractal structure is quantified by the complexity index coefficient, depicting some signs towards a multifractal simplification since 1990–1995 up to nowadays. It is also worth mentioning that the Hurst exponent, $H = h(q=2) - 1 \approx 0.5$, shows evidences of randomness both for Tmax and Tmin, being suggested a very slight tendency to an increase of H after year 2000.

As a summary, the changes in the thermometric regime at daily scale are quite evident, based on the calendar-day evolution and the multifractal structure, but an accurate quantification of the role played by the global warming induced by GHG emissions, the UHI phenomenon and the rise in population and urbanisation density should be the goal of future researches.

6 Conclusions

The analyses of a long series covering 102 years of daily maximum and minimum temperatures recorded at the Fabra Observatory (Barcelona), of verified good quality data, lead to:

- The computation of time trends and quantification of future extreme maximum and minimum calendar-day temperatures, with predominance of positive trends for Tmax and Tmin temperatures for most of calendar days. The largest significant positive trends are detected in autumn. Consequently, a future increase of the climatic summer length is to be expected. Additionally, the highest temperatures would be reached at the end of August and beginning of September.
- A complete multifractal analysis for the whole Tmax and Tmin data series has permitted a first evaluation of their multifractal structure. Additionally, the application of this multifractal analysis by using moving windows depicts the evolution of the multifractal complexity from the beginning to the end of the recording period. It is noticeable that the subsets of series evolve to low-complexity multifractal structure and some small signs of persistence, instead of randomness, are observed towards the end of the analysed period.

These results could represent a new insight into the behaviour of minimum and maximum calendar-day temperatures in Barcelona, one of the most densely populated urban areas of the Western Mediterranean, a geographical area greatly concerned in the context of climate change related hazards.

Acknowledgements Thermometric data recorded at Fabra Observatory have been obtained from the Royal Academy of Science and Arts (RACA, Barcelona).

Author contribution The three authors have contributed to computations, discussion of the results and writing of the manuscript.

Funding Open Access funding provided thanks to the CRUE-CSIC agreement with Springer Nature. This research has been financed by the project PID2019-105976RB-I00 (Agencia Estatal de Investigación, Spanish Government).

Data availability Thermometric data recorded at Fabra Observatory have been obtained from the Royal Academy of Science and Arts (RACA, Barcelona).

Code availability Codes for Mann–Kendall trends and MDFA algorithms have been created by the authors for the specific computations on the manuscript, taking as reference Sneyers (World Meteorological Office 1990) and Kantelhardt et al. (2002), respectively.

Declarations

Ethics approval Not applicable.

Consent to participate All authors consent to participate into the study.

Consent for publication All authors consent to publish the study in a journal article.

Conflict of interest The authors declare no competing interests.

References

Aggarwal SK, Lovallo M, Khan PK, Rastogi BK, Telesca L (2015) Multifractal detrended fluctuation analysis of magnitude series of seismicity of Kachchh region, Western India. Physica A 426:56–52. https://doi.org/10.1016/j.physa.2015.01.049

Aghakouchak A, Chiang F, Huning LS, Love ChA, Mallakpour I, Mazdiyasni O, Muftakhari H, Papalexiou SM, Ragno E, Sadegh M (2020) Climate extremes and compound hazards in a warming world. Annual Rev Earth Planet Sci 48:519–548. https://doi.org/10.1146/annurev-earth-071719-055228

Agliardi E, Alexopoulos T, Cech Ch (2019) On the relationship between GHGs and global temperature anomalies: multilevel rolling analysis and Copula calibration. Environ Resource Econ 72:109–133. https://doi.org/10.1007/s10640-018-0259-3

Altava-Ortiz, V., Barrera-Escoda, A. (2020): Escenaris climàtics regionalitzats a Catalunya (ESCAT-2020). Projeccions estadístiques regionalitzades a 1 km de resolució espacial (1971–2050). Informe tècnic. Servei Meteorològic de Catalunya, Departament de Territori i Sostenibilitat, Generalitat de Catalunya, Barcelona 169. https://www.meteo.cat/wpweb/climatologia/el-clima-dema/projeccions-de-temperatura-1971-2050/

Amengual A et al (2014) Projections of heat waves with high impact on human health in Europe. Glob Planet Change 119:71–84

Barrera-Escoda A, Gonçalves M, Guerreiro D, Cunillera J, Baldasano JM (2014) Projections of temperature and precipitation extremes in the North Western Mediterranean Basin by dynamical downscaling of climate scenarios at high resolution (1971–2050). Clim Change 122:567–582

Barros Pozo, P.M., Martín-Vide, J. (2018). Influencia térmica antrópica local y global en el observatorio Fabra para el periodo 1924–2016. BAGE, Bulletin of the Spanish Association of Geography 79. https://doi.org/10.21138/bage.2515a

Bensoussan N, Romano JC, Harmelin JG, Garrabou J (2010) High resolution characterization of northwest Mediterranean coastal waters thermal regimes: to better understand responses of benthic communities to climate change. Estuar Coast Shelf Sci 87:401–441

Bloomfield P (1992) Trends in global temperature. Clim Change 21:1–16

Burgueño A, Lana X, Serra C (2002) Significant hot and cold events at Fabra Observatory, Barcelona (NE Spain). Theoret Appl Climatol 71(3–4):141–156

Burgueño A, Lana X, Serra C, Martínez MD (2014) Daily extreme temperature multifractals in Catalonia (NE Spain). Phys Lett A 378:874–885

Corte-Real J, Zhang X, Wang X (1995) Large-scale circulation regimes and surface climatic anomalies over the Mediterranean. Int J Climatol 15:1135–1150. https://doi.org/10.1002/joc.3370151006

Cos J, Doblas-Reyes F, Jury M, Marcos R, Bretonnière P-A, Samsó M (2022) The Mediterranean climate change hotspot in the CMIP5 and CMIP6 projections. Earth Sys Dyn 13:321–340. https://doi.org/10.5194/esd-13-321-2022

Coumou D, Robinson A (2013) Historic and future increase in the global land area affected by monthly heat extremes. Environ Res Lett 8:034018. https://doi.org/10.1088/1748-9326/8/3/034018

Diffenbaugh NS, Pal JS, Giorgi F, Gao X (2007) Heat stress intensification in the Mediterranean climate change hotspot. Geophys Res Lett. https://doi.org/10.1029/2007GL030000

Diffenbaugh NS, Giorgi F (2012) Climate change hotspots in the CMIP5 global climatic model ensemble. Clim Change 114:813–822

Diffenbaugh NS, Singh D, Mankin JS, Horton DE, Swain DL, Touma D, Charland A, Liu Y, Haugen M, Tsiang M, Rajaratman B (2017) Quantifying the influence of global warming on unprecedent extreme climate events. Proc Natl Acad Sci USA 114:4881. https://doi.org/10.1073/pnas.1618082114

Fan X, Lin M (2017) Multiscale multifractal detrended fluctuation analysis of earthquake magnitude series of Southern California. Physica A 479:225–235. https://doi.org/10.1016/j.physa.2017.03.003

Founda D (2011) Evolution of the air temperature in Athens and evidence of climatic change: a review. Adv Build Energy Res 5:7–41. https://doi.org/10.1080/17512549.2011.582338

Hao X, Ruihong Y, Zhuangzhuang Z, Zhen Q, Xixi L, Tingxi L, Ruizhong G (2021) Greenhouse gas emissions from the water–air interface of a grassland river: a case study of the Xilin River. Sci Rep 11:2659

Giannakopoulos C, Le Sager P, Bindi M, Moriondo M, Kostopoulou E, Goodess CM (2009) Climatic changes and associated impacts in the Mediterranean resulting from a 2 °C global warming. Glob Planet Change 68:209–224

LA Gil-Alana 2009 Persistence and time trends in the temperatures in Spain AdvMeteorol Article ID 415290https://doi.org/10.1155/2009/415290

Gil-Alana LA, Sauci L (2019) Temperature across Europe: evidence of time trends. Clim Change 157:355–364

Gonçalves M, Barrera-Escoda A, Guerreiro D, Baldasano JM, Cunillera J (2014) Seasonal to yearly assessment of temperature and precipitation trends in the North Western Mediterranean Basin by dynamical dowscaling of climate scenarios at high resolution (1971–2050). Clim Change 122:243–256

IPCC, 2021: Climate Change 2021: The Physical Science Basis. Contribution of Working Group I to the Sixth Assessment Report of the Intergovernmental Panel on Climate Change [Masson-Delmotte, V., P. Zhai, A. Pirani, S.L. Connors, C. Péan, S. Berger, N. Caud, Y. Chen, L. Goldfarb, M.I. Gomis, M. Huang, K. Leitzell, E. Lonnoy, J.B.R. Matthews, T.K. Maycock, T. Waterfield, O. Yelekçi, R. Yu, and B. Zhou (eds.)]. Cambridge University Press. In Press.

IPCC, 2022: Climate Change 2022: Mitigation of Climate Change. Contribution of Working Group III to the Sixth Assessment Report of the Intergovernmental Panel on Climate Change. Cambridge University Press, Cambridge, UK and New York, NY, USA. https://doi.org/10.1017/9781009157926

Jones PD, Moberg A (2003) Hemispheric and large-scale surface air temperature variations: an extensive revision and an update to 2001. J Clim 16:206–223

Kantelhardt JW, Zschiegner SA, Koscielny-Bunde A, Havlin S, Bunde A, Stanley HE (2002) Multifractal detrended fluctuation analysis of nonstationary time series". Phys A Stat Mech App 316:87–114

Kutiel H, Maheras P (1998) Variations in the temperature regime across the Mediterranean during the last century and their relationship with circulation indices. Theoret Appl Climatol 61:39–53

La Sorte FA, Johnston A, Ault TR (2021) Global trends in the frequency and duration of temperature extremes. Clim Change 121. https://doi.org/10.1007/s10584-021-03094-0

Lana X, Martínez MD, Burgueño A, Serra C (2009) Statistics of hot and cold events in Catalonia (NE Spain) for the recording period 1950–2004. Theoret Appl Climatol 97:135–150

Lana X, Burgueño A, Serra C, Martínez MD (2015) Fractal structure and predictive strategy of the daily extreme temperature residual at Fabra Observatory (NE Spain, years 1917–2005). Theoret Appl Climatol 121:225–241. https://doi.org/10.1007/s00704-014-1236-6

Lana X, Rodríguez-Solà R, Martinez MD, Casas-Castillo MC, Serra C, Kirchner R (2020) Multifractal structure of the monthly rainfall regime in Catalonia NE Spain evaluation of the non-linear structural complexity of the monthly rainfall. CHAOS Interdisciplinary J Nonlinear Sci 30:7. https://doi.org/10.1063/5.0010342

H. Le Treut, R. Somerville, U. Cubasch, Y. Ding, C. Mauritzen, A. Mokssit, T. Peterson and M. Prather. (2007). Historical overview of climate change. In: Climate Change 2007: The Physical Science Basis. Contribution of Working Group I to the Fourth Assessment Report of the Intergovernmental Panel on Climate Change [Solomon, S., D. Qin, M. Manning, Z. Chen, M. Marquis, K.B. Averyt, M. Tignor and H.L. Miller (eds.)]. Cambridge University Press, Cambridge, United Kingdom and New York, NY, USA.

Lionello P, Scarascia L (2018) The relation between climate change in the Mediterranean region and global warming. Reg Environ Change 18:1481–1493

Lorenzo N, Díaz-Poso A, Royé D (2021) Heatwave intensity on the Iberian Peninsula: future climate projections. Atmos Res 258:105655

J Martin-Vide MC Moreno-Garcia 2020 Probability values for the intensity of Barcelona's urban heat island (Spain) Atmos Res 240 https://doi.org/10.1016/j.atmosres.2020.104877.ISSN:0169-8095

Martínez MD, Serra C, Burgueño A, Lana X (2010) Time trends of daily maximum and minimum temperatures in Catalonia (NE Spain) for the period 1975–2004. Int J Climatol 30:267–290

Meinshausen M, Vogel E, Nauels A, Lorbacher K, Meinshausen N, Etheridge DM, Fraser PJ, Montzka SA, Rayner PJ, Trudinger CM, Krummel PB, Beyerle U, Canadell JG, Daniel JS, Enting IJ, Law RM, Lunder CR, O'Doherty S, Prinn RG, Reimann S, Rubino M, Velders GJM, Vollmer MK, Wang RHJ, Weiss R (2017) Historical greenhouse gas concentrations for climate modelling (CMIP6). Geosci Model Dev 10:2057–2116. https://doi.org/10.5194/gmd-10-2057-2017

Monterrubio-Velasco, M., Lana, X., Martínez, M.D. Zúñiga, R. and de la Puente, J. (2020). Evolution of the multifractal parameters along different steps of a seismic activity. The example of Canterbury 2000–2018 (New Zealand). AIP Advances. https://doi.org/10.1063/5.0010103.

Moreno-Garcia, M.C. (1994). Intensity and form of the urban heat island in Barcelona. Int J Climatol 10/1002.joc.3370140609

Paeth H, Vogt G, Paxian A, Hertig E, Seubert S, Jacobeit J (2017) Quantifying the evidence of climate change in the light of uncertainty exemplified by the Mediterranean hot spot region. Glob Planet Change 151:144–151

Pausas JG, Fernández-Muñoz S (2012) Fire regime changes in the Western Mediterranean Basin: from fuel-limited to drought-driven fire regime. Clim Change 110:215–226

QueredaSala J, GilOlcina A, PerezCuevas A, OlcinaCantos J, RicoAmoros A, MontónChiva E (2000) Climatic warming in the Spanish Mediterranean: natural trend or urban effect. Clim Chang 46:473–483. https://doi.org/10.1023/A:1005688608044

Russo S, Sillmann J, Fischer EM (2015) top ten European heatwaves since 1950 and their occurrence in the coming decades. Environ Res Lett 10(12):124003. https://doi.org/10.1088/1748-9326/10/12/124003

Salvati A, Coch Roura H, Cecere C (2017) Assessing the urban heat island and its energy impact on residential buildings in Mediterranean climate: Barcelona case study. Energy Build 146:38–54. https://doi.org/10.1016/j.enbuild.2017.04.025

Serra C, Burgueño A, Lana X (2001) Analysis of maximum and minimum daily temperatures recorded at Fabra observatory (Barcelona, NE Spain) in the period 1917–1988. Int J Climatol 21(5):617–636

Serra C, Lana X, Martínez MD, Roca J, Arellano B, Biere R, Moix M, Burgueño A (2020) Air temperature in Barcelona metropolitan area from MODIS satellite and GIS data. Theoret Appl Climatol 139:473–492. https://doi.org/10.1007/s00704-019-02973-y

Shimizu Y, Thurner S, Ehrenberger K (2002) Multifractal spectra as a measure of complexity human posture. Fractals 10:104–116

Sigró J, Brunet M, Aguilar E, Saladie O, López D (2005) Spatial and temporal patterns of north-eastern Spain temperature change and their relationships with atmospheric and SST modes of variability over the period 1950–1998. Geophys Res Abstr 7(04118):1–2

Smith ET, Sheridan SC (2019) The influence of extreme cold events on mortality in the United States. Sci Total Environ 647:342–351. https://doi.org/10.1016/j.scitotenv.2018.07.466

Tuel A, Eltahir EAB (2020) Why is the Mediterranean a climate change hot spot? J Clim 33:5829–5843. https://doi.org/10.1175/JCLI-D-19-0910.1

Sneyers, R. (1990). On the statistical analysis of series of observation. Technical Note 415, World meteorological Office, WMO, Geneva 192

Stern DI, Kaufmann RK (2000) Detecting a global warming signal in hemispheric temperature series: a structural time series analysis. Clim Change 47:411–438

DD Wheeler VL Harvey DE Atkinson RK Collins MJ Mills 2011 A climatology of cold air outbreaks over North America: WACCM and ERA-40 comparison and analysis. J Geophys Res Atmosphere 116. https://doi.org/10.1029/2011JD015711

Wigley TML, Santer BD (2013) A probabilistic quantification of the anthropogenic component of twentieth century global warning. Clim Dyn 40:1087–1102. https://doi.org/10.1007/s00382-012-1525-8

Xoplaki E, González-Rouco JF, Luterbacher J, Wanner H (2003) Mediterranean summer air temperature variability and its connection to the large-scale atmospheric circulation and SSTs. Clim Dyn 20:723–739. https://doi.org/10.1007/s00382-003-0304-x

Zickfeld K, MacDougall AH, Matthews HD (2016) On the proportionality between global temperature change and cumulative CO_2 emissions during periods of net negative CO_2 emissions. Environ Res Lett 11:055006. https://doi.org/10.1088/1748-9326/11/5/055006